CHEMISTRY OF MATERIALS

ARTICLE

pubs.acs.org/cm

One-Step Melt Synthesis of Water-Soluble, Photoluminescent, Surface-Oxidized Silicon Nanoparticles for Cellular Imaging Applications

Beth A. Manhat,[†] Anna L. Brown,[†] Labe A. Black,[‡] J. B. Alexander Ross,[‡] Katye Fichter,[§] Tania Vu,[§] Erik Richman,[⊥] and Andrea M. Goforth*[,†]

[†]Department of Chemistry, Portland State University, Portland, Oregon 97201, United States

[‡]Department of Chemistry and Biochemistry, The University of Montana, Missoula, Montana 59812, United States

[§]Department of Biomedical Engineering, Oregon Health and Science University, Portland, Oregon 97239, United States

[⊥]Materials Science Institute, University of Oregon, Eugene, Oregon 97403, United States

Supporting Information

ABSTRACT: We have developed a versatile, one-step melt synthesis of water-soluble, highly emissive silicon nanoparticles using bifunctional, low-melting solids (such as glutaric acid) as reaction media. Characterization through transmission electron microscopy, selected area electron diffraction, X-ray photoelectron spectroscopy, and Raman spectroscopy shows that the one-step melt synthesis produces nanoscale Si cores surrounded by a silicon oxide shell. Analysis of the nanoparticle surface using FT-IR, zeta potential, and gel electrophoresis indicates that the bifunctional ligand used in the one-step synthesis is grafted onto the nanoparticle, which allows for tuning of the particle surface charge, solubility, and functionality. Photoluminescence spectra of the as-prepared glutaric acid-synthesized silicon nanoparticles show an intense blue−green emission with a short (ns) lifetime suitable for biological imaging. These nanoparticles are found to be stable in biological media and have been used to examine cellular uptake and distribution in live N2a cells.

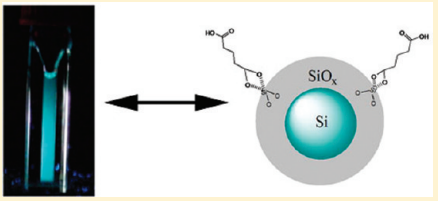

KEYWORDS: nanoparticles, silicon, Si nanoparticles, one-step synthesis, melt synthesis, surface modification, surface oxide, aqueous suspension, luminescence, quantum yield, optical spectroscopy, cellular imaging

INTRODUCTION

Semiconductor nanoparticles (NPs) have received widespread interest for their efficiency in tunable wavelength light emission, which has led to increased application of luminescent NPs in opto-electronic devices[1,2] and biological fluorescence imaging.[3,4] Considerable synthetic efforts have been placed on optimizing direct band gap II−VI semiconductor quantum dots (QDs), especially those based on Cd^{2+}, for such applications, owing to their high luminescence quantum yields (QY) and tunable visible emissions, which are governed by a size-dependent quantum confinement effect.[5−7] However, the electrochemical reactivity of binary QDs, as well as the biological toxicity of cadmium are concerning,[8,9] especially for intended use in aqueous, biological imaging applications. To overcome these limitations, inorganic shells (e.g., ZnS, SiO_2) are often added to binary Cd−chalcogenide QDs to decrease toxicity,[10] provide a measure of electrochemical stability,[11] and preserve or enhance fluorescence properties.[11] Furthermore, these QDs are often surface-stabilized by electrostatically or datively associated ligands.[3] Synthetic procedures for producing core/shell QDs are therefore multistep, an issue given that QD photophysical properties are very sensitive to preparation. Further complicating applications of II−VI QDs, noncovalently bound surface groups are proving to be non-ideal for biological applications due to equilibrium-mediated exchange,[12] usually resulting in the need for addition of a polymer coating that further increases QD size and complexity.

Since the discovery of intense photoluminescence from porous silicon (Si) in the early 1990s,[13] nanostructured Si has been studied as an efficient light emitter, though the origins of this photoluminescence are still vigorously debated. Nonetheless, luminescent, freestanding Si or silicon-based (e.g., oxidized Si) nanoparticles (NPs) have the potential to overcome the aforementioned issues associated with using II−VI semiconductor QDs as biological fluorophores. Because Si has already been established as a biocompatible element[14,15] and because covalent surface manipulations to impart various chemical functionalities on an Si surface are well-documented,[16,17] Si-based fluorophores are attractive for use in biological imaging applications. Furthermore Si is the foremost technologically relevant element in electronics applications, and careful development of Si-based fluorophores with controlled properties could also lead to increased applications of luminescent Si nanostructures in Si-based opto-electronics.[18] Several previous studies have demonstrated that Si-based nanoparticles exhibit high photoluminescence

Received: January 26, 2011
Revised: March 24, 2011
Published: April 14, 2011

QYs, which are comparable to those of both organic fluorophores and Cd-based QDs.[19]

To date, several methods have been presented to achieve matrix compatible, surface-functionalized Si NPs, including high- (solid state)[20,21] and low-temperature (solution)[22−24] methods, electrochemical[25] and plasma methods,[19,26,27] and supercritical fluid[28] and deposition[29] techniques. While most of these synthetic routes are at least two-step methods involving core synthesis and surface-capping steps, both laser synthesis in reactive vapor[30] and mechano-chemical methods in liquid ligands[31,32] have recently been found to produce luminescent, surface-capped Si NPs in a single step. However, these methods are not ideal for aqueous applications, as they have primarily led to NPs with hydrophobic surface terminations. Solution methods may be preferred, as they can theoretically produce particles with more variability and biocompatibility of surface terminating groups. Unfortunately, solution methods, including the reduction of SiX_4 (X = halide) in microemulsions[33,34] and Zintl salt metathesis[24,35] or oxidation,[36,37] have commonly required two steps to obtain water-soluble Si NPs. These reactions initially involve the generation of Si NP cores bearing a reactive Si−H or Si−X surface followed by subsequent reaction steps, including hydrosilylation or Grignard reactions, for Si-surface manipulation to impart the NPs with the desired matrix compatibility properties. Recently, water-soluble, oxide-embedded Si NPs were inadvertently produced in a single, solution-based reaction step.[38] However, it is clear from the report that the intention was to produce hydrophobic Si NPs by surface manipulation of Si−Br bonds using a previously reported Zintl salt oxidation/alkoxylation two-step method.[36] For such materials, attachment of suitable ligands to enable their use as biological fluorophores would require additional reaction steps to further derivatize the silicon oxide surface.

Herein, we report the one-step synthesis of hydrophilic, photoluminescent, oxide-embedded Si nanoparticles using a novel melt procedure, which employs a neat, low melting dicarboxylic acid solid as a low-volume solvent and potential direct surface modifier in the NH_4Br metathesis of the Zintl salt NaSi. The versatility of this reaction is important if the bifunctional melt medium interacts with the NP surface, which our results suggest, and therefore we demonstrate that the particles can be synthesized in numerous bifunctional solid melts or liquid solvents having a variety of chemical functional groups. Additionally, we demonstrate the facile uptake of these luminescent Si nanoparticles into live neuron cells with preservation of the photophysical properties; we observe that these emissive nanoparticles, which have fast, nanosecond radiative lifetimes, are internalized and evenly distributed throughout the cytoplasm. Finally, the melt method limits the number of synthetic steps, as well as the number and quantity of chemicals, used to synthesize Si nanoparticle colloids. Therefore, this method is relatively environmentally friendly when compared to traditional wet chemical syntheses, which often require hazardous HF etching procedures or large volumes of organic solvents.

EXPERIMENTAL SECTION

Materials. All synthetic manipulations were performed either in a nitrogen-filled glovebox or under an inert (Ar) atmosphere using standard Schlenk techniques. All aqueous solutions were prepared using electrophoretically pure water (nanopure water, 18 MOhm·cm resistivity). Prior to use, sodium silicide (NaSi, SIGNa, 80%) was ball milled for 15 min under N_2 in a tungsten carbide-lined milling vial with two 1-cm tungsten carbide balls using a high energy mill mixer (Spex 8000M). Ammonium bromide (NH_4Br, Aldrich, > 99.99%) and glutaric acid ($C_5H_8O_4$, Aldrich, 99%) were dried in vacuo at 100 °C before use. Anhydrous citric acid ($C_6H_8O_7$, Fisher, 99.5%), anhydrous ethylenediamine ($C_2H_8N_2$, Fisher, 98%), glutathione ($C_{10}H_{17}N_3O_6S$, Acros, 98%), or polyethylene glycol 200 ($H(OCH_2CH_2)_nOH$, Sigma, M_r = 190−210) were used as received in place of solid glutaric acid. It should be noted that despite measures to prevent exposure of reagents and products to adventitious oxygen, the mass balance of the NaSi starting material (80% purity) is silica and/or sodium silicates.[39] Our control experiments have indicated that this silicate-encapsulated NaSi starting material gives the same synthetic results as NaSi freshly prepared by solid state reaction of the elements. It should be noted that although the commercially available 80% NaSi we used is specially developed to be *less reactive* in air, metal silicides are in general flammable when exposed to air or moisture, and silicate-encapsulated NaSi is no exception. Thus, reactions were kept air and moisture free until complete reaction of NaSi was achieved, after which, the products were worked up in water and air.

Synthesis of Si NPs in a Neat Glutaric Acid Melt. In a typical reaction, NaSi (9.8 mmol), NH_4Br (19 mmol), and glutaric acid (GA, 114 mmol) were loaded into a two-neck, round-bottomed flask inside an N_2-filled glovebox. The closed reaction vessel was subsequently transferred to the Schlenk line, where the reaction mixture was heated to melt the GA (95−98 °C); the mixture was then brought to reflux (200 °C) for approximately 20 h, during which time a black suspension formed. After cooling to room temperature, the suspension solidified in unreacted GA; nanopure water (ca. 40 mL) was then added over the duration of 1 h with constant stirring to yield a black aqueous mixture. The black solid was removed by air-free vacuum filtration, leaving a yellow-colored solution containing the Si NPs. The black solid was identified as bulk, crystalline silicon by powder X-ray diffraction. The yellow Si NP solution was purified prior to analytical characterization as described below. Qualitatively, the results of the NaSi/NH_4X (X = halide) Zintl salt metathesis are the same if other ammonium halide salts (e.g., NH_4Cl, NH_4I) are used; similarly, NaSi/NH_4X ratios from 1:1 to 1:10 produce qualitatively similar Si NP products. A full exploration of the range and effect of reagent stoichiometry is beyond the scope of this paper.

To estimate the percent yield of silicon nanoparticles from this synthesis, the fluorescent, aqueous product was analyzed for Si content by ICP-MS. The percent yield of nanoparticles based on silicon, determined in this way, was 1%, which, assuming 4-nm particles with the density of bulk Si, is approximately 10^{15} nanoparticles/mL. Though the mass yield of fluorescent nanoparticles is relatively low, it is sufficient to purify, characterize, and utilize the NPs at concentrations appropriate for cellular imaging. The ICP-MS analysis was performed by a contracted lab (Dr. Martine Ralle, Oregon Health & Science University), using a sample and dilutions of known volumes.

Synthesis of Si NPs in Other Neat, Bi- or Multifunctional Ligands. Because of the possibility of directly tuning the Si NP surface chemistry by chemical or physical sorption of the bi- or multifunctional, low melting solid on the NP surface, silicon NPs were also synthesized in citric acid (CA) or glutathione (GSA) melts by substituting the neat solid for GA in the above procedure. Additionally, the neat, bi- or multifunctional liquids, ethylenediamine (en) or polyethylene glycol (PEG), were also used in the reaction in place of GA in the same relative molar quantities (1 NaSi/2 NH_4Br/10 ligand). All synthetic procedures in alternate solvents are similar to those described above for the synthesis of Si NPs in glutaric acid.

Purification of Si NPs Synthesized from a Neat Glutaric Acid Melt. Following isolation of the Si NPs in water, purification and analysis steps were performed in air. Excess GA and inorganic salts may be removed from the Si NP products by a combination of sublimation

and dialysis. Silica column chromatography of the as-prepared samples, which were taken to dryness and redissolved in chloroform before column loading, was not as effective in separating excess GA from the Si NPs as was sublimation/dialysis purification. To remove GA, the water-soluble products were taken to dryness by rotary evaporation and the resulting solid was subsequently subjected to sublimation using a coldfinger (containing dry ice/acetone) vacuum apparatus on the Schlenk line. The sample was heated to the reduced boiling point of GA and left under dynamic vacuum for up to 3 h; over time, a white solid was observed on the coldfinger, which was subsequently identified as neat, unreacted GA by ^{1}H NMR analysis. To reduce the amount of inorganic salts (NaBr formed during reaction or unreacted NH_4Br) in the aqueous Si NP solution, dialysis against nanopure water was performed up to three times using Fisher Brand hydrophilic dialysis tubing (regenerated cellulose, MWCO 1000 Da). Powder X-ray diffraction was used to identify crystalline solids left after evaporation of the dialysate, which were primarily NaBr but also contained some GA. Powder X-ray diffraction was also used to confirm the presence of Si^0 domains in the aqueous, fluorescent NP samples. These samples were prepared by drop-casting purified (by dialysis and sublimation), aqueous products onto a Pt sample holder to deposit a thin film.

^{1}H Nuclear Magnetic Resonance (^{1}H NMR) Spectroscopy and Powder X-ray Diffraction (PXRD). ^{1}H NMR and PXRD were used to identify solution and solid products after synthesis and purification steps. ^{1}H NMR in $CDCl_3$ or D_2O were recorded on a Bruker 400 mHz NMR spectrometer; PXRD measurements were made on a Rigaku Ultima IV X-ray diffraction system.

Analytical Characterization of Si NPs. The Si NP products of the glutaric acid melt synthesis were characterized by TEM, EDS, XPS, Raman spectroscopy, UV−visible spectrophotometry, photoluminescence spectrophotometry, cellular imaging, FT-IR, gel electrophoresis and zeta potential measurements. Sample preparations and measurements were done in air using samples originating as purified, aqueous colloids of the Si NPs unless otherwise noted. Measurements made on "as-prepared" samples refer to specimens prepared from aqueous colloids of the Si NPs prior to purification steps. Prior to the measurements, the aqueous colloids were stored in air, for as little as one day and up to several weeks. Electrophoretic mobility measurements were also performed on the Si NPs isolated from the citric acid- and ethylenediamine-mediated syntheses in order to compare the surface characteristics of Si NPs originating from different bi/multifunctional solvents. Si NPs synthesized in all of the neat solvents mentioned above were also characterized by photoluminescence spectrophotometry and the spectral characteristics in each case were similar to those of the Si NPs synthesized from the GA melt, showing only subtle changes in the position of lambda max at identical excitation wavelengths.

Transmission Electron Microscopy (TEM), Energy Dispersive X-ray Spectroscopy (EDS), and Selected Area Electron Diffraction (SAED). TEM and EDS measurements, performed on a Tecnai F-20 HR-TEM operating at 200 kV, were used to assess the morphology, size, size distribution, and composition of the as-prepared, GA-synthesized Si NP samples. Topological EDS spectra for composition analysis were collected on isolated particles for 10 min with approximately 20% dead time between successive scans. Samples were prepared by drop casting diluted aliquots of aqueous Si NPs onto 400-mesh holey carbon-coated copper grids (SPI), which were subsequently dried in air at 100 °C overnight. NPs (1020) from different areas of the same grid were manually measured. It should be noted that HR-TEM and topological EDS revealed crystalline NP cores, rich in Si (vide infra). Further electron diffraction analysis and line-scanning EDS were performed to examine the phase and composition of the particles. TEM images of the citric acid- and ethylenediamine-synthesized Si NPs were also obtained.

Line-scanning EDS and SAED were performed on an FEI Titan 80-300 TEM operating at 300 kV. Samples were prepared by drop casting as-prepared aqueous Si NPs onto lacey carbon-coated copper grids (Ted Pella), followed by subsequent drying in air at 100 °C overnight. An EDS line scan was performed over a large, isolated Si NP (16 μs dwell time with 20 points collected over the 20-nm length scale) to monitor the relative atomic ratios of Si and O as a function of position across the particle.

Raman Spectroscopy, X-ray Photoelectron Spectroscopy (XPS), and Fourier Transform Infrared (FT-IR) Spectroscopy. Raman spectra were collected on a Micro-Raman spectrometer (Jobin-Yvon LabRAM HR800 UV with 532 nm laser). Samples were prepared by drop casting standards and freshly purified, GA-synthesized Si NP solutions onto carbon tape adhered to glass slides 24 h prior to data collection. XPS measurements were made on a ThermoFisher Escalab 250. Samples were prepared by drop casting an as-prepared Si NP solution onto a clean Cr substrate, which was allowed to dry under ambient conditions. Prior to the XPS measurement, the sample stood in air for several days. During the measurement, charge compensation was done with a flood gun and for analysis, the C 1s peak was used as an internal reference set to 284.8 eV. FT-IR spectra were collected on a Nicolet iS10 spectrometer using a diamond ATR attachment. Aqueous solutions of neat GA and purified Si NPs from the GA melt were drop cast onto the ATR crystal and the solvent was evaporated as necessary using a heat gun to deposit a film. Solid samples of Si NPs purified by sublimation were measured immediately after sublimation and, for comparison, approximately 2 weeks after sublimation.

Zeta Potential. Zeta potential measurements to examine nanoparticle surface charge as a function of pH were collected on a Malvern ZS-90 using Zeta-sizer folded capillary cells with gold electrodes. A solution of as-prepared Si NPs from GA- or citric acid-mediated syntheses was manually titrated with 0.1 M NaOH to obtain solutions with pH values ranging from 1.84 to 8.51. Conversely, as-prepared Si NPs synthesized in ethylenediamine were brought up in water and titrated with 0.1 M H_2SO_4 to obtain solutions in the pH range of 10.06−7.06.

Gel Electrophoresis. A 1% agarose gel was prepared using TAE buffer (40 mM tris buffer, 20 mM acetic acid, 1 mM EDTA, pH to 8.3 using NaOH) with the well comb positioned in the center of the gel mold. The gel was allowed to polymerize for 1 h and samples of GA-, citric acid-, or ethylenediamine-synthesized Si NP solutions in water (ranging in volume from 0.5 to 3 μL) were mixed with 5 μL of a 50% glycerol solution and loaded into the gel. The gel electrophoresis experiment was performed at a constant voltage (50 V) over 1 h, and the gel was subsequently imaged in a UV light box (302 nm excitation) equipped with digital camera.

UV−vis, Standard Photoluminescence, and Time-Resolved Photoluminescence Spectrophotometry. UV−vis absorption spectra (200−800 nm) were collected on a Shimadzu UV-2450 UV−vis spectrophotometer in a standard 1-cm quartz cuvette. Standard photoluminescence (PL) measurements were collected on a Shimadzu-RF5301PC spectrophotometer. The same solutions from the UV−vis experiments were subsequently used for the PL measurements. QY values for the Si NPs were obtained relative to a suitable organic fluorophore, 2-aminopyridine (QY = 60%), chosen on the basis of similarity in absorbance and emission characteristics of sample and standard.[40] For the analysis, 2-aminopyridine solutions were prepared in 0.1 M H_2SO_4 while the Si NPs were diluted in nanopure H_2O from the as-prepared concentration. Serial dilutions were made until a series with linear absorbance values at 350 nm were obtained for both sample and standard, such that the maximum absorbance value did not exceed 0.1. PL spectra were obtained for these dilutions using excitation at 350 nm and measuring the emission intensity in the wavelength range 360−900 nm. The integrated intensities of the PL emission spectra were plotted against the corresponding absorbance values and the slopes were used to determine the relative QYs. The absolute QY of the Si NPs

Scheme 1. One-Step Melt Synthesis of Si NPs in Glutaric Acid (Reagents, Solids; Products, Aqueous after Addition of Water to Solid Product)

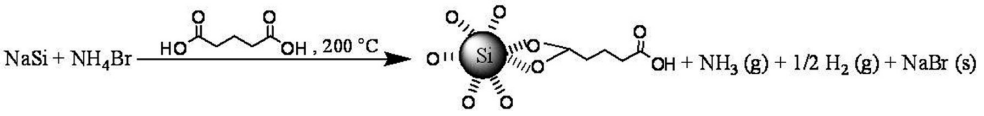

was subsequently calculated by multiplying the relative QY by the quantum efficiency of 2-aminopyridine, according to the following equation: $\Phi_x = \Phi_{ST}((\text{slope}_x)/(\text{slope}_{ST}))((\eta_x^2)/(\eta_{ST}^2))$.[40] Here, Φ is the quantum efficiency and η is the refractive index for the standard (ST) and sample (x) solutions, respectively. Time-resolved luminescence decay measurements were performed under magic-angle polarization conditions[41] by time-correlated single-photon counting (TCSPC) using the FLASC 1000 (Quantum Northwest, Liberty Lake, WA) sample chamber. A frequency-doubled, ps-Mira 900 Ti:Sapphire laser (Coherent, Santa Clara, CA) provided pulsed excitation at 375 nm and at a repetition rate of 4.7 MHz. The emission was isolated through 25-nm bandpass filters having peak transmission at 400, 435, 455, or 495 nm (Andover, Salem NH), respectively. Data were also collected using 400 nm excitation, with emission detected at 435, 455, and 495 nm. The TCSPC data were collected at a timing resolution of 35 ps/channel using a Time Harp 200 PCI board (PicoQuant, Berlin) and each intensity decay curve was collected to 4×10^4 at the peak. An instrument response function was also collected to equivalent peak counts, using a light-scattering solution of dilute colloidal silica.

It was assumed that the intensity decay, $I(t)$, could be adequately described by sums of exponentials. In this case, $I(t) = \sum_{i=1}^{n} \alpha_i e^{-t/\tau_i}$, where τ_i is the lifetime and α_i is the amplitude of the ith component in the intensity decay. The intensity-weighted lifetime is then $\langle\tau\rangle = \sum_{i=1}^{n} \alpha_i \tau_i^2 / \sum_{i=1}^{n} \alpha_i \tau_i$. The data were fit by nonlinear least-squares using iterative reconvolution (software package FluoFit Pro V4.2.1 (PicoQuant, Berlin)), and the statistical goodness of fits was assessed by the reduced chi squared value, randomness of the residuals, and autocorrelation of the residuals.[41,42]

Cellular Imaging. GA-synthesized Si NPs were imaged using a neuroblastoma cell line derived from mice, Neuro-2a (N2a) (ATCC). Cells were cultured in a medium composed of 47.5% Dulbecco's Modified Eagle's Medium (D-MEM), 47.5% Opti-MEM, and 5% fetal bovine serum (FBS). Two days prior to imaging, cells were plated at a 40 000 cell/well density in a 6-well plate and protected by a 25-mm poly-D-lysine clover slip. To examine the cellular uptake, the medium was removed and replaced with a concentrated sample of GA-synthesized Si NPs (1 mL/well) in PBS (pH = 7.4). The cells were then incubated in the NP solution for 1 h at 37 °C before washing the cells 2−3 times with PBS. The cells were imaged on a Zeiss Axiovert 200 M inverted microscope fitted with a 100× objective (NA = 1.4) using a QD525 filter set from Chroma (Rockingham, VT) with a 400 ± 60-nm excitation filter, a 475-nm long pass dichroic filter, and a 525 ± 40-nm emission filter. Z-stack images of live N2a cells were acquired in both differential interference contrast (DIC) and emission modes using a monochrome CCD Axiocam camera. The spacing between each slice was 275 nm. Control cells (without the addition of Si NPs) were also imaged in the same way.

RESULTS AND DISCUSSION

One-Step Synthesis of Hydrophilic Si NPs in Neat, Bi-, or Multifunctional Ligand Melts. Inspired by the conventional Zintl metathesis reaction between metal silicide and ammonium halide solids,[24,43,44] the one-step synthesis method we have developed utilizes low-melting, bi-, or multifunctional organic solids to serve as both the reaction medium (upon melting) and prospective surface terminating group (Scheme 1). Briefly, when NaSi, NH_4Br, and glutaric acid (GA = $HOOC(CH_2)_3COOH$) are reacted in a 1:2:10 molar ratio, the resulting luminescent nano-Si product is immediately soluble, without further manipulation, in water and aqueous buffers. The synthesis method is general and versatile as it can be performed in numerous bi- or multifunctional, low-melting solids (e.g., glutathione, other polypeptides, other di- or poly carboxylic acids), low-melting or liquid polymers (e.g., PEG), or in small volumes of neat, liquid ligands (e.g., ethylenediamine) using the same relative stoichiometry of reagents as in the GA reaction. The reaction proceeds equally well in all O- or N-donor media, even in monodentate O- or N-donor ligand solvents, but it does not produce luminescent NPs when purely aliphatic or aromatic solvents (e.g., xylene) are used in place of GA.

Previously, Kauzlarich and others have used the metal silicide metathesis reaction to generate Si NPs in *N*,*N*-dimethylformamide, dioctylether, and dimethoxyethane (MSi/solvent, where M = alkali metal, in 1:70 or greater molar ratios) and have reported that at least some fraction of the NPs bear reactive Si−H surfaces, as evidenced by FT-IR spectroscopy.[35] These Si NPs can be kept stable in organic media by hydrosilylation with long-chain alkenes or alkynes, or they can be functionalized for water solubility with functionalized alkenes or by coating alkylated Si particles with an amphiphilic polymer (e.g., alkyl-grafted poly(acrylic acid)).[24] These methods of imparting long-term matrix compatibility and solubility have required multistep syntheses to generate luminescent, surface functionalized Si NPs, and, according to the results herein, have required larger volumes of organic solvents than are apparently needed.

Additionally, if water-soluble particles are desired, a second surface-termination step following the initial core generating reaction step seems unnecessary in light of the results we present as well as those recently reported by Lin et al. In the latter,[38] a surface manipulation step to impart hydrophobicity was used following a metal silicide oxidation reaction; however, after the surface-capping reaction, the luminescent particles were found to be inherently water-soluble. The unintended oxide-coated particles generated in this preparation, alongside our unsuccessful syntheses in nondonor solvents, are taken as evidence that there is an implied role of a coordinating atom in the NP formation step, which we elaborate upon below. Despite the fact that only a monodentate solvent medium is required for the one-step synthesis of water-soluble Si NPs, an advantage of using multifunctional media (e.g., diamines, dicarboxylic acids), according to our electrophoretic mobility results (vide infra), is that a second functionality may be available at the Si NP/solvent interface for further surface manipulation steps, e.g., adding a biological marker of interest.

Characterization of Hydrophilic, Luminescent Si NPs from the One-Step Melt Synthesis in GA. Representative TEM

dx.doi.org/10.1021/cm200270d |*Chem. Mater.* 2011, 23, 2407–2418

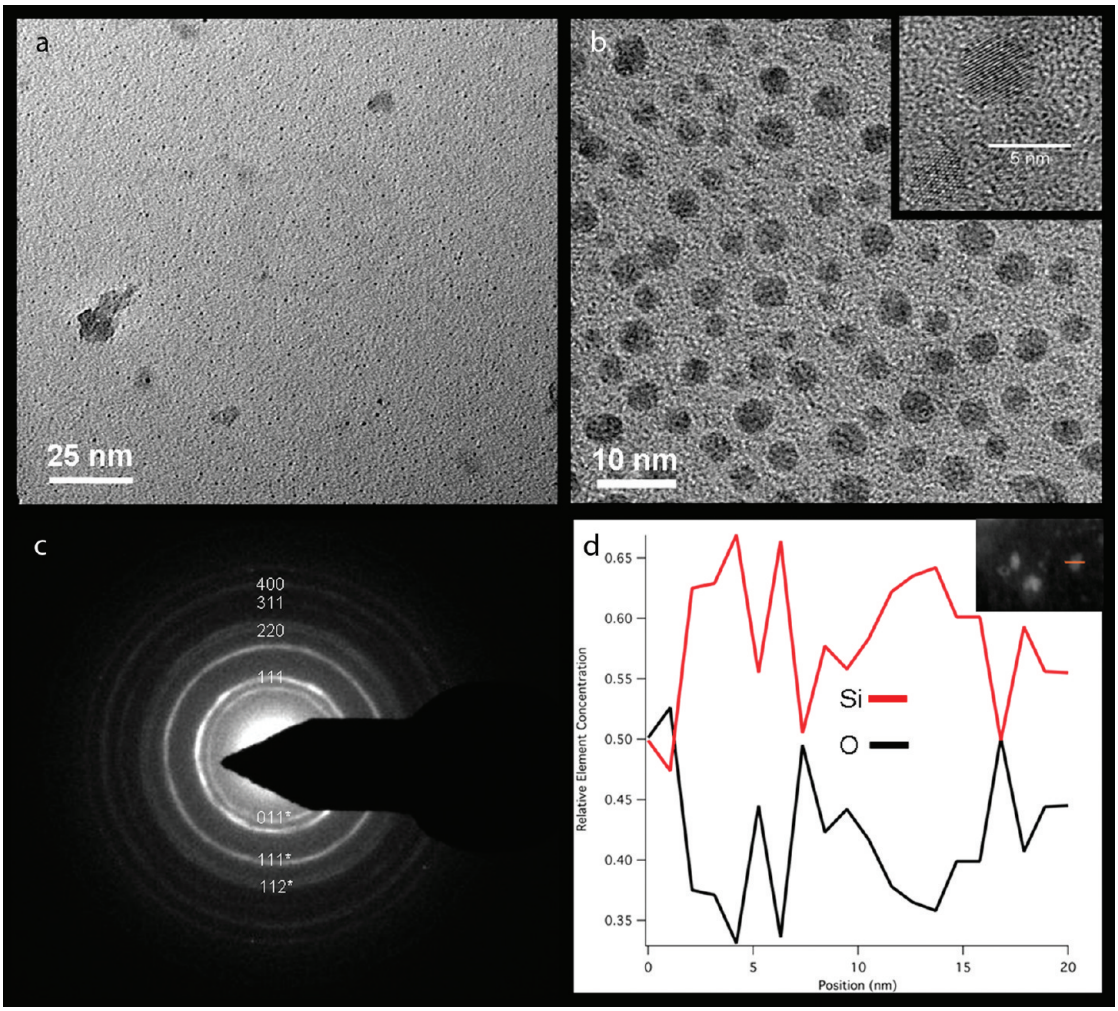

Figure 1. (a,b) TEM images of GA-synthesized Si NPs showing well-dispersed, spherical particles, scale bars 25 (a) and 10 nm (b). (Inset b) HR-TEM image showing a high degree of crystallinity in the NP cores, scale bar 5 nm. (c) SAED pattern of NPs showing the corresponding diamond Si and SiO_2 (*) diffraction rings. (d) EDS line scan monitoring the relative O and Si concentrations across a particle, suggesting oxidized surfaces and Si^0 rich cores. (Inset d) dark field TEM image of isolated NP on which EDS line scan was performed, scale bar 20 nm.

images of the one-step, melt-synthesized Si NPs prepared in GA are shown in Figure 1a and b; the particles produced by this method appear spherical, abundant, and are relatively monodisperse. Measuring 1020 NPs from various areas of the TEM grid, the particles were determined to be 3.9 ± 0.8 nm (see histogram in Supporting Information (SI), Figure S1); thus the majority of the NPs are smaller than the Bohr exciton radius of Si.[34] TEM images of citric acid (CA)- and ethylenediamine (en)-synthesized Si NPs are shown in Figure S2; those prepared in CA and en were of similar size to those prepared in GA, 5.7 ± 1.1 nm and 3.9 ± 0.9 nm, respectively, which suggests that the one-step synthesis method yields consistently small, fairly monodisperse Si NPs.

HR-TEM (inset, Figure 1b) indicates that the Si NP cores are crystalline, but indexing lattice fringes exhibited by these particles to diamond lattice Si was not straightforward. Similar issues have been encountered for other oxide-embedded crystalline Si NPs and are attributed to forced invasive oxidation and lattice strain.[45] However the SAED pattern (Figure 1c) shows multiple rings consistent with diamond lattice Si[46] ((111) at 3.14 Å, (220) at 1.92 Å, (311) at 1.64 Å, and (400) at 1.34 Å; JCPDS card 35-118). In addition, other diffraction rings observed at 3.4 Å, 2.1 Å and 1.8 Å (marked with *) are consistent with SiO_2 (JCPDS card 087-2096; (011) at 3.3 Å, (111) at 2.1 Å, and (112) at 1.8 Å). This result is attributed to the partial oxidation of the Si NPs, which are potentially capped with an oxygen-containing organic material, surface oxide, surface hydroxide, or a combination of these.

Energy dispersive X-ray spectroscopy (SI Figure S3) on the purified NP products revealed the elements Si, O, C, Cu (grid), and small amounts of Na and Br (starting material and salt byproduct). The high counts from C and O are expected: from the Cu grid coating (C), from adventitious atmosphere (O), from unreacted GA that may remain after purification (C and O), or from GA bound to Si NPs (C and O). Therefore, the presence of C and O observed by EDS does not indicate any particular mode of GA−NP association. A subsequent EDS line scan, 20 nm long, was performed over a large, isolated Si NP (inset, Figure 1d) to monitor the relative atomic ratios of Si and O as a function of position across the particle. These measurements (Figure 1d) indicate an O/Si ratio far less than 2:1 (expected for pure SiO_2), and in general, far less than 1:1, which suggests Si^0 rich regions.

dx.doi.org/10.1021/cm200270d |*Chem. Mater.* 2011, 23, 2407–2418

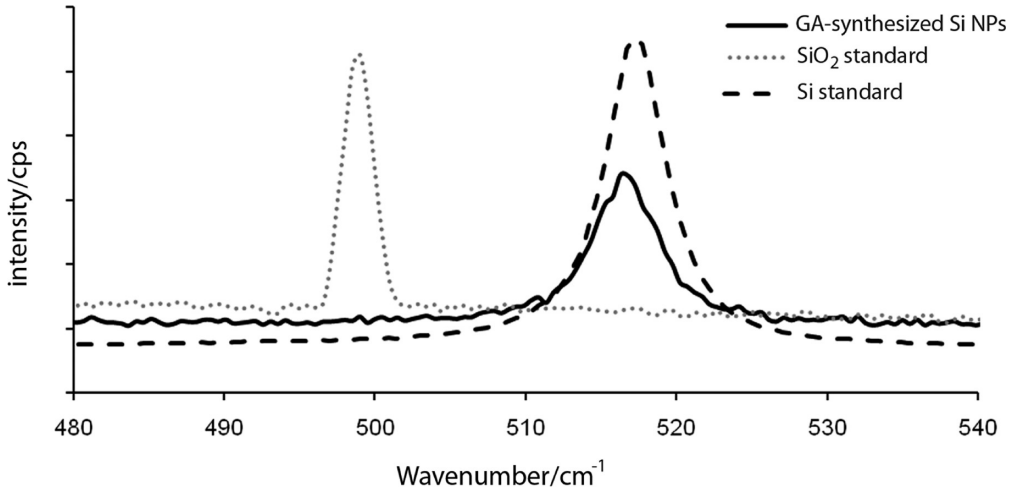

Figure 2. Raman spectra of freshly prepared GA-synthesized Si NPs (black solid) compared to SiO_2 (gray dotted) and Si (black dashed) standards, confirming that the NP sample contains elemental Si domains.

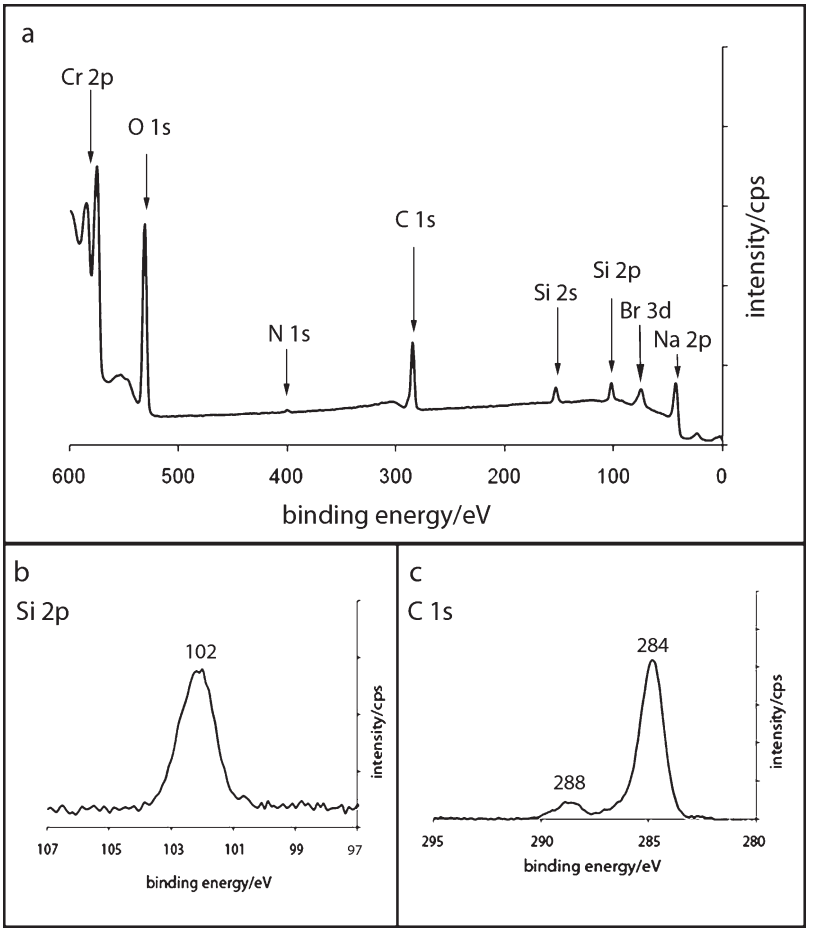

Figure 3. (a) XPS survey scan of aged GA-synthesized Si NPs detecting primarily Si, O, C, and Cr (foil). (b) Si 2p region with one peak centered at ~102 eV, indicating an SiO_x surface assignment. (c) C 1s region showing two peaks at 284 and 288 eV from adventitious carbon and carboxylate species, respectively.

Furthermore, as the beam was swept across the particle, the measured O/Si ratios generally did not approach 1 until the edges of the NP were reached, suggesting that the surfaces are more heavily oxidized than the cores. To further examine the nature of the particle core and surface, Raman, X-ray photoelectron, and FT-IR spectroscopies were also performed.

Raman spectroscopy was performed on a macroscopic sample of freshly purified GA-synthesized Si NPs (Figure 2). The

maximum of the vibration band is found at 515.2 cm^{-1} for the Si NP sample, which is close to the Si−Si vibration from bulk, crystalline Si at 516 cm^{-1}.[30] This slight blue shift, which has been previously observed for other Si NPs,[30] is attributed to the smaller domain size in nano-Si. The SiO_2 standard exhibits a vibration centered at 498 cm^{-1}. The Si NPs do not exhibit a peak in this region, which suggests the absence of silicon oxide in the freshly prepared sample. According to our XPS and FT-IR results (see below), we expect that an Si−O feature would appear in time with the increase in surface oxidation. However, unlike the FT-IR measurements, this measurement was not repeated after aging the purified Si NPs. To verify the presence of Si^0 domains observed by Raman spectroscopy, powder X-ray diffraction analysis (Figure S4) was performed on a drop-casted film, prepared using a purified aqueous Si NP sample obtained from a GA melt. The X-ray diffraction pattern shows the expected reflections corresponding to the (111) and (220) planes of diamond lattice Si (at 28.12 and 47.12 degrees 2-θ, respectively), in good agreement with the corresponding calculated pattern (at 28.47 and 47.34 degrees 2-θ, respectively). These peaks are weak in intensity relative to those of the sample holder; thus higher angle reflections are not visible above noise and we did not estimate the crystallite size based on line broadening.

XPS analysis was conducted and the survey scan detected the presence of Si, C, O, Br, and Cr (foil) as shown in Figure 3a. Upon close inspection of the Si 2p region (Figure 3b), the single, broad Si peak was assigned as SiO_x ($x < 2$) based on the absence of loss features expected for crystalline Si (99 eV);[47] the calibrated, energetic position of the Si 2p peak was found to be ~102 eV. It is unlikely that charging was an issue in accurately determining the Si 2p binding energy, and therefore GA-synthesized Si NPs are assigned an SiO_x surface, which is further supported by the separation between the C 1s and Si 2p signals. This separation should be approximately 186 eV assuming that the C 1s signal at 284.8 eV is dominated by adventitious carbon.[48] Here, the separation between the C 1s and the Si 2p signal was found to be slightly less than 183 eV, suggesting that the calibrated position of the Si 2p peak was ~102 eV, again, indicative of SiO_x. The results of the XPS are consistent with a high level of oxidation on the Si NP surface as are the results of SAED and EDS analyses. Additionally, the C 1s region of the XPS spectrum (Figure 3c) also shows a peak at 288 eV, consistent with carboxylate carbon.[49] Therefore, the collective results support the hypothesis that small, crystalline Si^0 regions are present in the core of the particles and are surrounded by an oxidized silicon surface on which the solvent has, to some extent, adsorbed. With the Si NPs larger than the expected mean free path of the ejected electrons,[50] absence of crystalline Si loss features is not unexpected given that the Si^0 regions might not be detected because they are deeply embedded.

To further examine the nature of the NP surface and to examine the role of the ligand solvent more closely, FT-IR spectroscopy, zeta potential, and gel electrophoresis techniques were used. Because the freshly prepared Raman sample revealed no oxidized silicon and the aged XPS sample revealed no Si^0, FT-IR was also used to examine the effects of prolonged air exposure. The FT-IR spectra (600−1800 cm^{-1}) of neat GA, freshly purified GA-synthesized Si NPs, and aged purified GA-synthesized Si NPs are shown in Figure 4 (full spectra, 400−4000 cm^{-1}, Figure S5). To provide surface coverage and minimize surface energy upon NP formation, it was anticipated that the ligand solvent, GA, would covalently bond to the Si

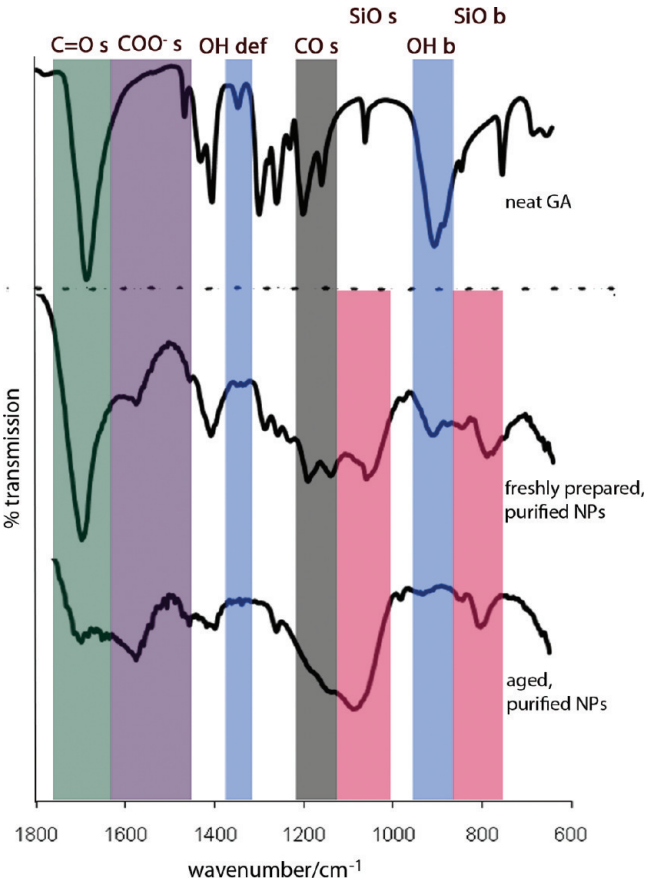

Figure 4. Fingerprint regions of the FT-IR spectra for neat GA (top), freshly prepared, purified Si NPs (middle), and aged, purified Si NPs (bottom). The sample spectra show characteristics of surface bound bidentate carboxylate in addition to surface oxidation, which increases over time.

or SiO_x NP surface. For each potentially surface-bound GA molecule, steric arguments would suggest that one −COOH group would interact with the NP surface, leaving the other group at the NP/solvent interface available to interact with other particles or available for subsequent functional group manipulations (e.g., peptide addition by carbodiimide coupling). Therefore, a change in the carbonyl region (relative to neat GA) would be expected for the GA-synthesized Si NPs if GA were covalently bound to the Si or SiO_x surface through one or more of its acid groups. The carbonyl region of the Si NP spectrum (shaded in green) is broadened and split (from 1680 to 1700 and 1575 cm^{-1} [shaded in purple]) relative to that of neat GA, which may indicate a change in the ligand C═O environment. Similar spectroscopic features have been observed previously in the carbonyl regions of other samples with carboxylated surfaces, including carboxy-terminated Ge (100) 2 × 1 surfaces,[51] carboxylic acid-grafted silica NPs,[52] and other carboxy-terminated Si NPs.[22] In the latter report, a shift of the carbonyl signal to 1600 cm^{-1} occurred upon covalent carboxylic acid attachment, similar to the shift to 1575 cm^{-1} observed in the case of our particles; thus, our FT-IR results are supportive of GA interacting with the NP surface in a bidentate manner. In addition, Kim et al. report the appearance of an Si−O−C vibration at 1083 cm^{-1},[52] which should also be present in our product spectra if GA is covalently bound to the NPs. In the Si NP product spectrum, there is a strong, broad peak in that region, centered at

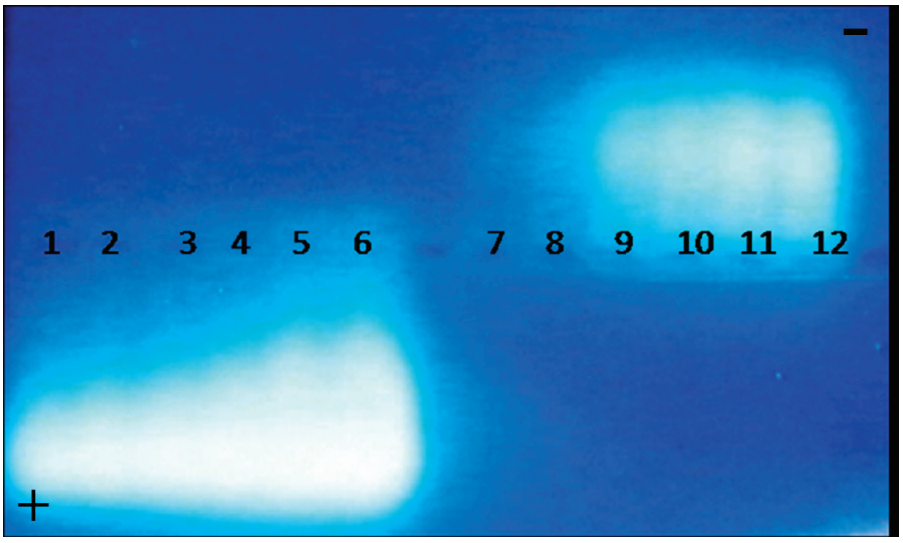

Figure 5. Digital image of agarose gel under 302 nm light after electrophoresis of the luminescent Si NPs. Left to right: wells 1−6, increasing concentrations of (−)-charged CA-synthesized Si NPs; wells 7−12, increasing concentrations of (+)-charged en-synthesized Si NPs. The positions and charges of the electrodes are indicated as (+) or (−).

1077 cm^{-1} as well as a Si−O bend[53] at 800 cm^{-1} (shaded in pink). These peaks are consistent with an Si−O species, especially with partially oxidized Si NPs; however, the two possibilities (Si−O−C or Si−O) cannot be differentiated due to the broad nature of the Si−O stretch. These features both increase in magnitude upon aging the sample in air, suggestive of increasing oxidization of the surface with time. Regardless of the initial surface passivation, which may be a mixture of covalent GA, oxide, or hydroxide, this growth suggests that Si NPs eventually exhibit a heavily oxidized surface. Curiously, the −OH vibrations (shaded in blue) at 1372 and 917 cm^{-1} are found to decrease with increased levels of oxidation. While the split carboxylate region suggests at least partial surface coverage by GA, the breadth of the Si−O peak at 1077 cm^{-1} precludes definitive assignment of a surface grafted Si−O−C feature. Therefore, zeta potential measurements and gel electrophoresis of oppositely charged CA- and en- synthesized Si NP samples were compared to examine the possible solvent molecule surface grafting.

Zeta potential measurements were made on a series of aqueous CA-synthesized and en-synthesized Si NPs at varying pHs to compare the surface charge characteristics, indicative of the identity of surface bound species, of Si NPs originating from different bifunctional solvents. As shown in Figure S6, Si NPs synthesized in CA exhibit a gradually increasing *negative* potential when titrated to higher pH due to the increasing partial deprotonation of the carboxylic acid groups at pH > pK_a ($pK_{a(1)}$ of CA is 3.13). Conversely, en-synthesized Si NPs have an increasing *positive* zeta potential when titrated to a lower pH, which is consistent with the increasing number of charged $-NH_3^+$ groups when pH < pK_a ($pK_{a(1)}$ of en is 10.08). These results are consistent with the electrophoretic mobility results of Mahalingam et al.[54] and indicate the ability of the one-step melt synthesis to chemically vary the Si NP surface charge via the variation in the identity of the ligand solvent. To corroborate the differing surface charges of the Si NPs, gel electrophoresis was performed. Because the Si NPs are emissive, staining or processing steps were not necessary to image the gel. Figure 5 shows the migration of CA- and en-synthesized Si NPs to be consistent with the zeta potential results: CA-synthesized NPs migrate toward the positive electrode, suggesting that they are *negatively* charged, while the en-synthesized NPs migrate toward the negative electrode, suggesting that they are *positively* charged. The electrophoretic mobility behavior of negatively charged, GA-synthesized Si NPs is similar to that of the CA-synthesized Si NPs. Thus, based on all the analytical evidence, it seems most likely that our particles consist of Si^0 nanocrystals residing in an oxide matrix and covered by surface-bound solvent molecules that do not completely passivate the surface, allowing it to become increasingly oxidized with time.

Photophysical Properties of Hydrophilic, Luminescent Si NPs from the One-Step Melt Synthesis in GA. The photophysical properties of the hydrophilic, luminescent Si NPs from the one-step synthesis in GA were studied. Figure 6 shows the photoluminescence (a) and absorption spectra (b) of the GA-synthesized Si NPs in water. Absorption spectra were collected on a series of dilutions of the Si NP solution, and on an aqueous solution of neat GA. Neat GA does not absorb in the visible while the solution of Si NPs has an onset of absorbance at approximately 500 nm with a distinct shoulder that peaks at about 350 nm. The long absorption tail is consistent with the indirect bandgap character of Si while the shoulder at ∼350 nm (3.5 eV) has been associated with Si direct bandgap transitions.[34,55] Both of these features have been observed in the absorption spectra for Si NPs of similar size.[24,55,56]

The emission spectra of the as-prepared, aqueous Si NP colloid were collected using a series of excitation wavelengths ranging from 310 to 520 nm in 30 nm intervals (see SI Figure S7 for spectra collected at all excitation wavelengths). As a control, an aqueous sample of GA of concentration similar to that used in the synthesis was measured; it was not luminescent. The Si NP solution has an emission maximum at 502 nm when excited at 460 nm, and the excitation wavelength dependence of the emission observed for the sample is typical of previously reported blue-emitting Si NPs;[24,31,36,57−59] this spectroscopic behavoir is generally attributed to size polydispersity and the excitation of different sized NPs with different λ_{ex}. The quantum yield of the Si NPs in aqueous solution was calculated as described in the

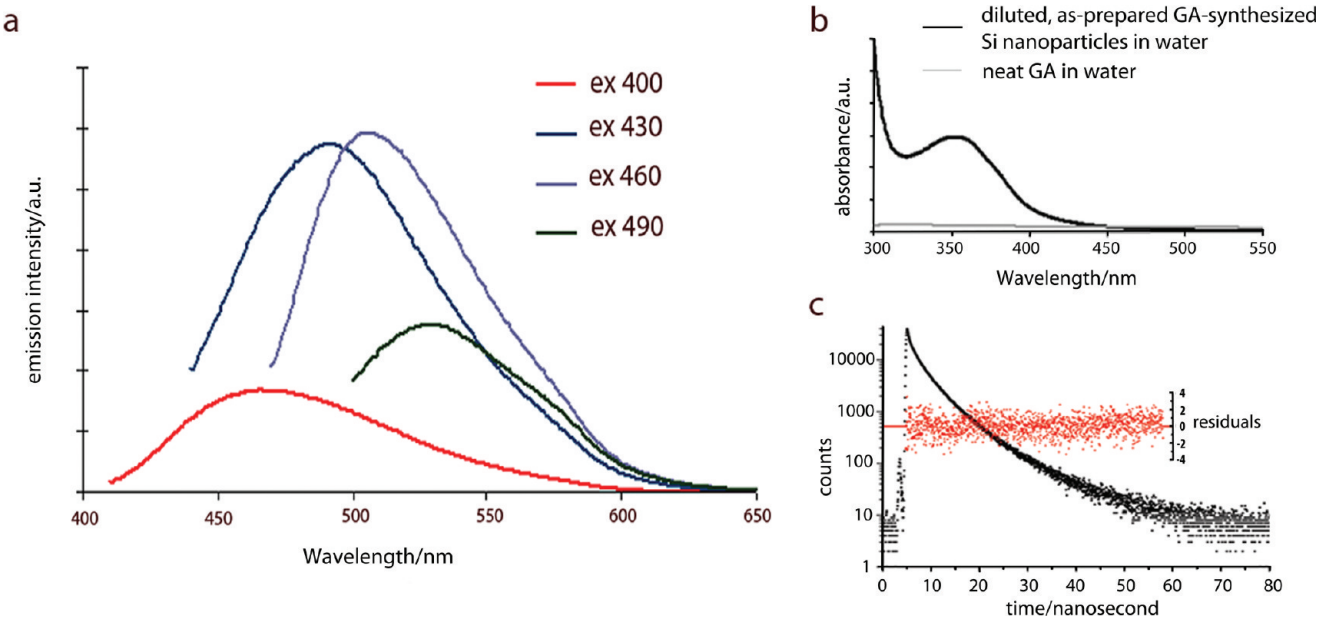

Figure 6. (a) Emission spectra of GA-synthesized Si NPs in H_2O excited at 400 (red), 430 (dark blue), 460 (light blue) or 490 nm (green). (b) UV−vis absorption spectra of neat GA (gray) and Si NPs synthesized via the one-step melt synthesis in GA (black). (c) Time-resolved emission spectrum of GA-synthesized Si NPs in H_2O excited at 375 nm. Emission was monitored at 455 nm; the intensity weighted lifetime was determined to be 3.6 ns. The inset shows the residuals of the experimental curve fit, which results in a flat difference line.

Experimental section. Determined relative to 2-aminopyridine, it is 13(1)%, which is comparable to QY values reported for other Si NP colloids prepared by solution methods.[60−62] The photophysical properties of the Si NPs were found to be stable over time, as spectroscopic measurements taken after several months of storage under ambient conditions were identical to those of freshly prepared samples. PL spectra of Si NPs produced in variations of the one-step method in alternate ligand solvents are found in SI (Figure S8). All samples synthesized by the one-step method in neat ligands are emissive in water, with maxima ranging between 440 and 550 nm when excited between 370 and 430 nm; in all cases, the emission peak shifts to longer wavelength with excitation at longer wavelength. Regardless of the melt medium used in the one-step synthesis, QY values are similar to those of GA-synthesized samples, e.g., the QY of the citric acid-synthesized Si NPs was found to be 12%. It is also noteworthy that all Si NP products synthesized in ligand melts are luminescent upon formation, prior to the addition of water and prior to exposure to atmosphere; previously, Si NP luminescence was reported to develop only after the addition of water.[4]

The origin of photoluminescence in nanostructured Si is an ongoing discussion in the literature[55] due to the possibility of radiative events occurring from delocalized core states (given that crystalline Si^0 domains are present to generate exciton pairs) or from localized states arising from surface, interface, or shell defects.[17,18,34,63] Further complicating elucidation of luminescence mechanism, Si NPs are readily oxidized, which results in Si^0 core shrinkage and blue-shifting band gap recombination pathways;[46] as a result, the emission wavelength is sensitive to sample age and processing.[46,63] Additionally, luminescent self-trapped excitons, as well as luminescent defect states, have been observed in pure SiO_2 and silicon suboxides,[64−66] and the possibility of these can complicate the assignment of luminescent states in heavily oxidized Si nanostructures, such as those in this work.

It has been reported that 4-nm Si particles, such as these we report herein, emit in the red region of the visible spectrum due to the electron−hole recombination across the direct bandgap, consistent with expectations of quantum confinement.[17] However, it has been determined both theoretically[67] and experimentally[68] that surface states, in addition to quantum-confined states, markedly influence Si NP optical properties, and Si NPs in the quantum-confined regime that are embedded in oxide matrices have been reported to exhibit both a blue and a red emission event.[68−70] It has been suggested that these coexistent emissions may be observed due to competing decay pathways of core-generated excitons.[29,63,71] In these systems, the red emission is attributed to quantum-confined, direct band gap transitions while the blue emission is attributed to exciton recombination at localized defect states at the oxide interface or in the oxide shell.[63,68,69] The 4(±1)-nm Si nanoparticles synthesized by the one-step melt method exhibit only an intense blue emission, suggesting that emission from defect states dominates the photophysical behavior, unless, due to high levels of oxidation, the Si NP cores are very small and the quantum-confinement related emission event is strongly blue-shifted. However, blue−green emission has also been observed from amorphous silica nanostructures lacking an Si^0 component, but, in order to observe this, excitation wavelengths shorter than 250 nm or short, time-pulsed excitations are generally necessary.[65,66] These instrumental conditions were not used in our routine spectroscopic experiments, suggesting that pure SiO_x-based electronic transitions are not responsible for the observed blue emission from the as-synthesized Si NPs. Thus, the blue luminescence we observe from our oxide-embedded Si NPs may be attributed to either the quantum-confined state of ultrasmall (∼1−2 nm) Si nanocrystals or to radiative recombination of core-generated excitons at surface or shell defects.

Because O-associated surfaces on Si nanocrystals have been reported to act as radiative centers for the exciton pairs to

dx.doi.org/10.1021/cm200270d |*Chem. Mater.* 2011, 23, 2407–2418

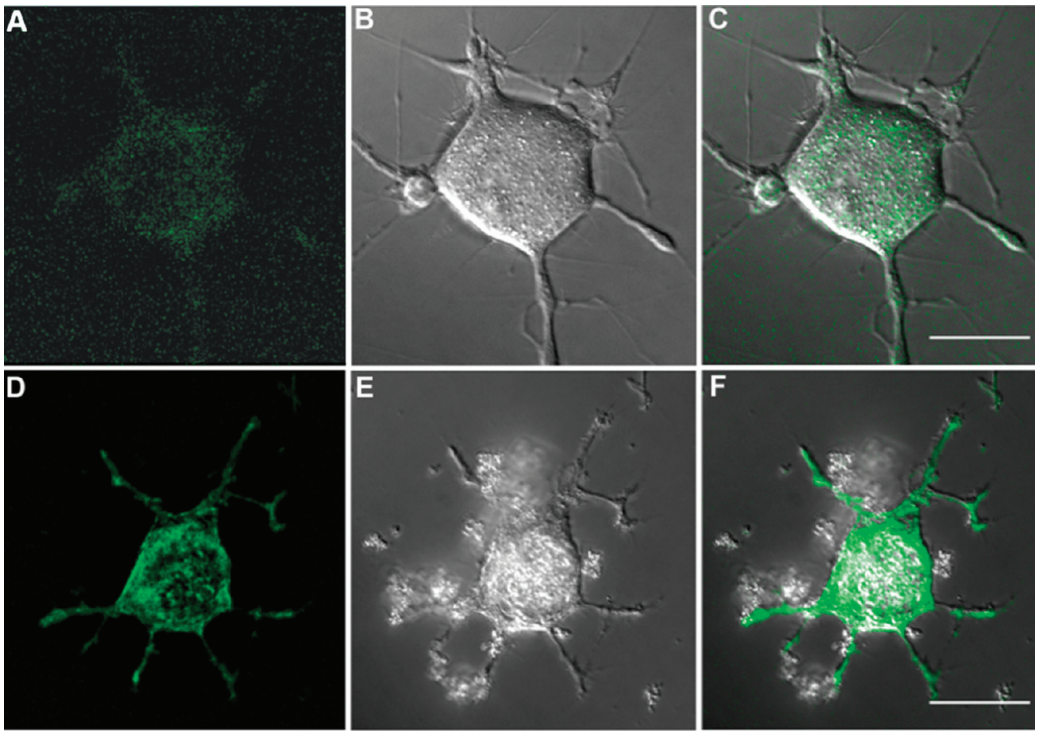

Figure 7. GA-synthesized Si NPs incubated with N2a cells for 1 h to monitor cellular uptake. Fluorescence images of live N2a cells for control (a, no luminescent Si NPs added) and experimental (d, fluorescent Si NPs added) specimens. DIC images show the outline of the cell structure in control (b) and experimental (e) cells. Overlay of the fluorescence and optical images of control (c) and experimental (f) cells. Scale bars = 10 μm.

recombine with very short lifetimes (ps−ns), as opposed to longer lived excited states characteristic of direct (ns−ms) or indirect gap states (μs−ms),[34,46,64,71,72] we also examined the lifetime of the blue photoluminescence. When both red and blue emissions are observed for oxide-embedded Si NPs, the longer-lived red event has generally been attributed to quantum confinement while the shorter-lived blue event has been attributed to oxygen-centered luminescence from localized states, which act as recombination centers for core-generated excitons.[63,69,71] The lifetime data of the GA-synthesized Si NPs (Figure 5c) indicates a multiexponential decay when excited at 375 nm and monitored at 455 nm. Under these conditions, the intensity-weighted average lifetime was 3.6 ns, consistent with the time-scale of defect-related emission from small (<3 nm) Si nanocrystals in oxide matrices.[71] However, it should be noted that as the physical dimensions of the nanocrystal are reduced, carrier recombination becomes more facile, resulting in shorter lifetimes,[34,69] and making it more difficult to discern differences between band gap and defect transitions in smaller Si nanocrystals. Because SAED, topological EDS, and Raman measurements support the existence of Si^0 domains in samples that are luminescent prior to water addition and extensive oxidation, and because the particles are, in general, no larger than 5 nm *including* the oxide shell, the blue, ns-lifetime luminescence we observe is also consistent with exciton decay from quantum confined states. Supportive of this, similar blue emission characteristics have been observed for other small Si nanoparticles with O-associated surfaces, including alcohols[73] and carboxylic acids,[22,74] and are attributed to quantum confinement.[72,75] However, because the lifetimes of direct gap and defect-related emissions are reported to be similar in very small Si nanocrystals,[69,71] the value of lifetime alone cannot be used to distinguish the two phenomena and the wavelength dependence of lifetime should be considered.

When emission was monitored at other wavelengths (400 and 495 nm, data not shown), modest changes in lifetime were observed (intensity weighted averages of 3.2 and 3.7 ns, respectively); this slight wavelength dependence of lifetime may reflect the polydispersity in the Si particle size as relaxation rates are understood to be a size-dependent property. Modest increases in lifetime with increasing emission wavelength are also observed in other polydisperse, oxidized silicon nanostructures,[69,72] including porous Si, and this behavior has been regarded as indicative of quantum confinement since little wavelength dependence is expected for luminescent, localized states that are discrete in nature. However, the lifetime changes with changing wavelength are small, and thus, we cannot rule out exciton recombination at local states associated with the Si NP surface oxidation.

Regardless of the origin of the observed luminescence, the exceptional stability of the aqueous, luminescent Si NPs synthesized by this one-step method indicates the high potential for their use as biomedical fluorophores, which has been examined in our cellular uptake studies (Figure 7). The fast lifetimes of our water-soluble, highly luminescent Si NPs should be distinguishable from longer-lived cellular autofluorescence events, suggesting that these Si NPs may find utility as cellular imaging agents if they interact favorably in the cell environment. To investigate the affinity (or uptake) of the Si NPs toward a sample cell line, GA-synthesized particles were incubated with live mouse neuroblastoma cells (N2a) and emission intensity after washing was monitored at 525 nm (excitation at 400±60 nm). The control image (Figure 7a) shows minimal luminescence (mostly due to endogenous flavins) from the N2a cells relative to the N2a cells with the incorporated Si NPs (Figure 7d). Thus, the luminescence observed from the N2a cells arises from the Si NPs that

have been taken up into the cells. The bright signal is distributed evenly throughout the N2a cell, indicating that the negatively charged, luminescent particles were taken up into the cytoplasm with retention of their photophysical properties. Given that cellular uptake and distribution is dependent on charge, as well as motif recognition, the ability to modify the surface charge and functionality via our one-step synthesis method makes these Si NPs a versatile platform for development of more selective, targeted NP imaging agents in the future.

In summary, we have developed a versatile one-step, melt-synthesis method to produce water-soluble, photoluminescent silicon nanoparticles, which despite the high degree of surface oxidation, bear at least some surface-bound bifunctional solvent molecules. TEM studies indicate that this one-step method produces fairly monodisperse nanoparticles with little dependence on the identity of the ligand solvent and SAED revealed that these particles contain nanoscale Si^0 domains, which is additionally supported by Raman spectroscopy. All particles synthesized via the one-step synthesis method exhibit a bright photoluminescence in the blue region of the visible spectrum; the photoluminescence has a 3−4 ns lifetime. The ease and versatility of synthesis, the long-term aqueous stability of the NP products, and the extreme robustness of the photophysical properties make these Si NPs excellent candidates for biomedical applications, as demonstrated by the imaging of the glutaric acid-synthesized NPs in N2a cells.

■ ASSOCIATED CONTENT

Supporting Information. Size distribution histogram for GA-synthesized Si NPs, TEM images of CA- and en-synthesized Si NPs, energy dispersive X-ray spectrum of GA-synthesized Si NPs, XRD pattern of purified, GA-synthesized Si NPs, full FT-IR spectra of GA and GA-synthesized NP products, zeta potential titration data, and full photophysical characterization from all synthetic variations (PDF). This material is available free of charge via the Internet at http://pubs.acs.org.

■ AUTHOR INFORMATION

Corresponding Author
*E-mail: agoforth@pdx.edu.

■ ACKNOWLEDGMENT

We acknowledge Dr. Anne Bentley (Lewis & Clark College) for zeta potential access, Micah Eastman and Dr. Jun Jiao (Portland State University) for Raman spectroscopy access, and the Portland State University Center for Electron Microscopy and Nanofabrication for microscopy access. Financial support for this project was provided by the Burroughs Wellcome Fund (A.M.G., Award 1007294.01; A.M.G. holds a Career Award at the Scientific Interface from the Burroughs Wellcome Fund), the Oregon Nanoscience and Microtechnologies Institute (A.M.G., Signature Research Fellow, Task Order 3 of the Master Grant Agreement and T.V./A.M.G., ONAMI/ONR Award N000141010082), the United States Air Force (E.R., Award FA8650-05-1-5041), and the National Center for Research Resources (J.B.A.R., Award RR 15583). Finally, we thank the NSF for PXRD instrumentation (NSF-MRI, Award DMR-0923572).

■ REFERENCES

(1) Plass, R.; Pelet, S.; Krueger, J.; Grätzel, M.; Bach, U. *J. Phys. Chem. B* **2002**, *106*, 7578–7580.
(2) Baxter, J. B.; Aydil, E. S. *Appl. Phys. Lett.* **2005**, *86*, 053114.
(3) Gao, X. H.; Cui, Y. Y.; Levenson, R. M.; Chung, L. W. K.; Nie, S. M. *Nat. Biotechnol.* **2004**, *22*, 969.
(4) Park, J. H.; Gu, L.; von Maltzahn, G.; Ruoslahti, E.; Bhatia, S. N.; Sailor, M. J. *Nat. Mater.* **2009**, *8*, 331.
(5) Murray, C. B.; Norris, D. J.; Bawendi, M. G. *J. Am. Chem. Soc.* **1993**, *115*, 8706.
(6) Kim, S.; Fisher, B.; Eisler, H. J.; Bawendi, M. *J. Am. Chem. Soc.* **2003**, *125*, 11466.
(7) Alivisatos, A. P. *J. Phys. Chem.* **1996**, *100*, 13226.
(8) Kondoh, M.; Araragi, S.; Sato, K.; Higashimoto, M.; Takiguchi, M.; Sato, M. *Toxicology* **2002**, *170*, 111.
(9) Kirchner, C.; Liedl, T.; Kudera, S.; Pellegrino, T.; Javier, A. M.; Gaub, H. E.; Stolzle, S.; Fertig, N.; Parak, W. J. *Nano Lett.* **2005**, *5*, 331.
(10) Derfus, A. M.; Chan, W. C. W.; Bhatia, S. N. *Nano Lett.* **2004**, *4*, 11.
(11) Smith, A. M.; Nie, S. M. *Acc. Chem. Res.* **2010**, *43*, 190.
(12) Aldana, J.; Wang, Y. A.; Peng, X. G. *J. Am. Chem. Soc.* **2001**, *123*, 8844.
(13) Canham, L. T. *Appl. Phys. Lett.* **1990**, *57*, 1046.
(14) Stewart, M. P.; Buriak, J. M. *Adv. Mater.* **2000**, *12*, 859.
(15) Morse, D. E. *Trends Biotechnol.* **1999**, *17*, 230.
(16) Buriak, J. M. *Chem. Rev.* **2002**, *102*, 1271.
(17) Veinot, J. G. C. *Chem. Commun.* **2006**, 4160.
(18) Godefroo, S.; Hayne, M.; Jivanescu, M.; Stesmans, A.; Zacharias, M.; Lebedev, O. I.; Van Tendeloo, G.; Moshchalkov, V. V. *Nat. Nanotechnol.* **2008**, *3*, 174.
(19) Jurbergs, D.; Rogojina, E.; Mangolini, L.; Kortshagen, U. *Appl. Phys. Lett.* **2006**, *88*, 233116.
(20) Hessel, C. M.; Henderson, E. J.; Veinot, J. G. C. *Chem. Mater.* **2006**, *18*, 6139.
(21) Kravitz, K.; Kamyshny, A.; Gedanken, A.; Magdassi, S. *J. Solid State Chem.* **2010**, *183*, 1442.
(22) Rogozhina, E. V.; Eckhoff, D. A.; Gratton, E.; Braun, P. V. *J. Mater. Chem.* **2006**, *16*, 1421.
(23) Dhas, N. A.; Raj, C. P.; Gedanken, A. *Chem. Mater.* **1998**, *10*, 3278.
(24) Zhang, X. M.; Neiner, D.; Wang, S. Z.; Louie, A. Y.; Kauzlarich, S. M. *Nanotechnology* **2007**, *18*, 095601.
(25) Kang, Z. H.; Tsang, C. H. A.; Wong, N. B.; Zhang, Z. D.; Lee, S. T. *J. Am. Chem. Soc.* **2007**, *129*, 12090.
(26) Gupta, A.; Swihart, M. T.; Wiggers, H. *Adv. Funct. Mater.* **2009**, *19*, 696.
(27) Shen, P.; Uesawa, N.; Inasawa, S.; Yamaguchi, Y. *J. Mater. Chem.* **2010**, *20*, 1669.
(28) Holmes, J. D.; Ziegler, K. J.; Doty, R. C.; Pell, L. E.; Johnston, K. P.; Korgel, B. A. *J. Am. Chem. Soc.* **2001**, *123*, 3743.
(29) Ferraioli, L.; Wang, M.; Pucker, G.; Navarro-Urrios, D.; Daldosso, N.; Kompocholis, C.; Pavesi, L. *J. Nanomater.* **2007**, 43491.
(30) Shirahata, N.; Linford, M. R.; Furumi, S.; Pei, L.; Sakka, Y.; Gates, R. J.; Asplund, M. C. *Chem. Commun.* **2009**, *31*, 4684.
(31) Heintz, A. S.; Fink, M. J.; Mitchell, B. S. *Adv. Mater.* **2007**, *19*, 3984.
(32) Heintz, A. S.; Fink, M. J.; Mitchell, B. S. *Appl. Organometal. Chem.* **2010**, *24*, 236.
(33) Warner, J. H.; Rubinsztein-Dunlop, H.; Tilley, R. D. *J. Phys. Chem. B* **2005**, *109*, 19064.
(34) Wilcoxon, J. P.; Samara, G. A.; Provencio, P. N. *Phys. Rev. B* **1999**, *60*, 2704.
(35) Neiner, D.; Chiu, H. W.; Kauzlarich, S. M. *J. Am. Chem. Soc.* **2006**, *128*, 11016.
(36) Pettigrew, K. A.; Liu, Q.; Power, P. P.; Kauzlarich, S. M. *Chem. Mater.* **2003**, *15*, 4005.
(37) Liu, Q.; Kauzlarich, S. M. *Mater. Sci. Eng., B* **2002**, *96*, 72.

(38) Lin, S. W.; Chen, D. H. *Small* **2009**, *5*, 72.
(39) Dye, J. L.; Cram, K. D.; Urbin, S. A.; Redko, M. Y.; Jackson, J. E.; Lefenfeld, M. *J. Am. Chem. Soc.* **2005**, *127*, 9338.
(40) Yvon, H. J. *A Guide to Recording Fluorescence Quantum Yields*. http://www.horiba.com/fileadmin/uploads/Scientific/Documents/Fluorescence/quantumyieldstrad.pdf.
(41) Badea, M. G.; Brand, L. *Methods Enzymol.* **1979**, *61*, 378.
(42) Grinvald, A.; Steinberg, I. Z. *Anal. Biochem.* **1974**, *59*, 583.
(43) Neiner, D.; Kauzlarich, S. M. *Chem. Mater.* **2010**, *22*, 487.
(44) McMillan, P. F.; Gryko, J.; Bull, C.; Arledge, R.; Kenyon, A. J.; Cressey, B. A. *J. Solid State Chem.* **2005**, *178*, 937.
(45) Ray, M.; Jana, K.; Bandyopadhyay, N. R.; Hossain, S. M.; Navarro-Urrios, D.; Chattyopadhyay, P. P.; Green, M. A. *Solid State Commun.* **2009**, *149*, 352.
(46) Germanenko, I. N.; Dongol, M.; Pithawalla, Y. B.; El-Shall, M. S.; Carlisle, J. A. *Pure Appl. Chem.* **2000**, *72*, 245.
(47) Heitsch, A. T.; Hessel, C. M.; Akhavan, V. A.; Korgel, B. A. *Nano Lett.* **2009**, *9*, 3042.
(48) Wagner, C. D.; Naumkin, A. V.; Kraut-Vass, A.; Allison, J. W.; Powell, C. J.; Rumble, Jr., J. R. NIST X-ray Photoelectron Spectroscopy Database, Version 3.5; National Institute of Standards and Technology: Gaithersburg, MD, 2003.
(49) Feng, L. B.; Wang, Y. L.; Wang, N.; Ma, Y. X. *Polym. Bull.* **2009**, *63*, 313.
(50) Powell, C. J.; Jablonski, A. *J. Phys. Chem. Ref. Data* **1999**, *28*, 19.
(51) Filler, M. A.; Van Deventer, J. A.; Keung, A. J.; Bent, S. F. *J. Am. Chem. Soc.* **2006**, *128*, 770.
(52) Kim, S.; Kim, E.; Kim, W. *J. Colloid Interface Sci.* **2005**, *292*, 93.
(53) Kim, H. J.; Shao, Q.; Kim, Y. H. *Surf. Coat. Technol.* **2003**, *171*, 39.
(54) Mahalingam, V.; Onclin, S.; Peter, M.; Ravoo, B. J.; Huskens, J.; Reinhoudt, D. N. *Langmuir* **2004**, *20*, 11756.
(55) Kanemitsu, Y. *Phys. Rep.* **1995**, *263*, 1.
(56) Kanemitsu, Y. *Phys. Rev. B* **1994**, *49*, 16845.
(57) English, D. S.; Pell, L. E.; Yu, Z. H.; Barbara, P. F.; Korgel, B. A. *Nano Lett.* **2002**, *2*, 681.
(58) Belomoin, G.; Therrien, J.; Nayfeh, M. *Appl. Phys. Lett.* **2000**, *77*, 779.
(59) Zou, J.; Sanelle, P.; Pettigrew, K. A.; Kauzlarich, S. M. *J. Clust. Sci.* **2006**, *17*, 565.
(60) Kusova, K.; Cibulka, O.; Dohnalova, K.; Pelant, I.; Fucikova, A.; Valenta, J. *Physica E* **2009**, *41*, 982.
(61) Shirahata, N.; Hasegawa, T.; Sakka, Y.; Tsuruoka, T. *Small* **2010**, *6*, 915.
(62) Rosso-Vasic, M.; Spruijt, E.; van Lagen, B.; De Cola, L.; Zuilhof, H. *Small* **2008**, *4*, 1835.
(63) Qin, G. G.; Song, H. Z.; Zhang, B. R.; Lin, J.; Duan, J. Q.; Yao, G. Q. *Phys. Rev. B* **1996**, *54*, 2548.
(64) Kontkiewicz, A. J.; Kontkiewicz, A. M.; Siejka, J.; Sen, S.; Nowak, G.; Hoff, A. M.; Sakthivel, P.; Ahmed, K.; Mukherjee, P.; Witanachchi, S.; Lagowski, J. *Appl. Phys. Lett.* **1994**, *65*, 1436.
(65) Trukhin, A. N.; Goldberg, M.; Jansons, J.; Fitting, H. J.; Tale, I. A. *J. Non-Cryst. Solids* **1998**, *223*, 114.
(66) Shluger, A.; Stefanovich, E. *Phys. Rev. B* **1990**, *42*, 9664.
(67) Zhou, Z. Y.; Brus, L.; Friesner, R. *Nano Lett.* **2003**, *3*, 163.
(68) Hessel, C. M.; Henderson, E. J.; Kelly, J. A.; Cavell, R. G.; Sham, T. K.; Veinot, J. G. C. *J. Phys. Chem. C* **2008**, *112*, 14247.
(69) Bley, R. A.; Kauzlarich, S. M.; Davis, J. E.; Lee, H. W. H. *Chem. Mater.* **1996**, *8*, 1881.
(70) Tamura, H.; Ruckschloss, M.; Wirschem, T.; Veprek, S. *Appl. Phys. Lett.* **1994**, *65*, 1537.
(71) de Boer, W.; Timmerman, D.; Dohnalova, K.; Yassievich, I. N.; Zhang, H.; Buma, W. J.; Gregorkiewicz, T. *Nat. Nanotechnol.* **2010**, *5*, 878.
(72) Warner, J. H.; Hoshino, A.; Yamamoto, K.; Tilley, R. D. *Angew. Chem., Int. Ed.* **2005**, *44*, 4550.
(73) Shiohara, A.; Hanada, S.; Prabakar, S.; Fujioka, K.; Lim, T.; Yamamoto, K.; Northcote, P.; Tilley, R. D. *J. Am. Chem. Soc.* **2010**, *132*, 248.
(74) Sato, S.; Swihart, M. T. *Chem. Mater.* **2006**, *18*, 4083.
(75) Rosso-Vasic, M.; Spruijt, E.; Popovic, Z.; Overgaag, K.; van Lagen, B.; Grandidier, B.; Vanmaekelbergh, D.; Dominguez-Gutierrez, D.; De Cola, L.; Zuilhof, H. *J. Mater. Chem.* **2009**, *19*, 5926.